nature materials

LETTERS

PUBLISHED ONLINE: 12 AUGUST 2012 | DOI: 10.1038/NMAT3401

Quantum effect on thermally activated glide of dislocations

Laurent Proville[1], David Rodney[2]* and Mihai-Cosmin Marinica[1]

Crystal plasticity involves the motion of dislocations under stress. So far, atomistic simulations of this process have predicted Peierls stresses[1], the stress needed to overcome the crystal resistance in the absence of thermal fluctuations, of more than twice the experimental values, a discrepancy best-known in body-centred cubic crystals[2–4]. Here we show that a large contribution arises from the crystal zero-point vibrations, which ease dislocation motion below typically half the Debye temperature. Using Wigner's quantum transition state theory[5,6] in atomistic models of crystals, we found a large decrease of the kink-pair formation enthalpy due to the quantization of the crystal vibrational modes. Consequently, the flow stress predicted by Orowan's law[7] is strongly reduced when compared with its classical approximation and in much closer agreement with experiments. This work advocates that quantum mechanics should be accounted for in simulations of materials and not only at very low temperatures or in light-atom systems.

Crystals, simply because they are made of atoms, impose a resistance to the motion of their dislocations. This resistance is characterized by the so-called Peierls stress[1], measured experimentally as the zero-temperature limit of the flow stress of well-annealed crystals[8,9]. Depending on the dislocation core structure, the Peierls stress may be negligibly small, as for $a/2\langle 110\rangle\{111\}$ dislocations in face-centred cubic (fcc) crystals, but it may also be appreciably large, as for $a/2\langle 111\rangle$ screw dislocations in body-centred cubic (bcc) crystals. In the latter case, dislocation glide proceeds at low temperature through the Peierls mechanism, where thermal fluctuations in the crystal vibrations occasionally induce the nucleation of a pair of kinks on straight dislocations (Fig. 1). The kinks then glide at high velocity along the dislocation line, allowing the whole dislocation to advance to the next equilibrium position, called a Peierls valley.

Atomistic calculations of the Peierls stress have so far been based on classical mechanics. However, already in 1971, from early simulations of bcc sodium, it was reported that the Peierls stress of screw dislocations was 0.01μ (μ is the elastic shear modulus), much larger than experimental data, between 0.002 and 0.0033μ. Since then, similar discrepancies have been reported in a wide range of bcc crystals[3,10,11], notwithstanding the use of electronic structure methods to accurately represent atomic bonding[12,13] or boundary conditions adapted to dislocations[12,14]. In the case of bcc iron modelled in Fig. 1, the computed Peierls stress is 0.9 GPa (Fig. 2), compared with 0.4 GPa obtained experimentally[8,9]. Several theories have been proposed to explain this discrepancy, invoking collective dislocation dynamics[15] and dislocation junctions[16]. These processes are unquestionably at play during plastic flow, but they only partially solve the discrepancy because they are, for example, absent from recent low-temperature *in situ* observations[17], where the stress level remains small compared with atomistic simulations.

To reduce the thermal activation, the experiments to measure the Peierls stress are performed at low temperatures where quantum effects are possible. Dislocation zero-point vibration[3,4,18] and tunnelling[18,19] have been considered theoretically in phenomenological models where the dislocation is viewed as a single particle or an elastic string. These models, however, rely on a very simplified description of some essential features, particularly the atomistic structure of the dislocation core and the quantum dynamics of the crystal itself, and cannot provide a quantitative explanation for the discrepancy between simulated and experimental Peierls stresses. Here we apply a fully atomistic approach to analyse how quantum statistics contribute to the thermally activated glide of dislocations.

To address a specific case, we consider first an atomic model of bcc iron based on a recent many-body embedded atom method (EAM) interatomic potential[20], which provides a satisfactory description of the dislocation core geometry and glide process in comparison with electronic-structure first-principles calculations[21]. The latter method cannot be employed here because of the large number of atoms ($N = 123{,}120$) required to model kink pairs without strong finite-size effects. The case of bcc iron can be considered as prototypical of other bcc crystals where first-principles calculations show similar dislocation features[12,13]. Two examples of classical computation of the minimum enthalpy path for the nucleation and propagation of a kink pair on a screw dislocation are reported in Fig. 2a at different applied shear stresses τ_{yz}. The calculations are based on the nudged elastic band method (see ref. 22 and Methods section for details). The maximum along the paths is the activated state, consisting of a dislocation with a critical kink pair. The corresponding enthalpy, the kink-pair formation enthalpy H_{kp}, is plotted in Fig. 2b against τ_{yz}. As can be seen, the formation enthalpy falls down to zero at a stress limit of 0.9 GPa, which defines the classical Peierls stress for the present energy model.

The rate of barrier crossing, $\Gamma_{\mathrm{classic}}$, which controls the dislocation velocity $v = a\Gamma_{\mathrm{classic}}$ (a is the distance between Peierls valleys) can be expressed in classical mechanics using the harmonic transition state theory[23] (TST):

$$\Gamma_{\mathrm{classic}} = L\sqrt{\frac{2\pi m}{kT}}\frac{\prod_{i=1}^{3N-3}\nu_i^{\mathrm{init}}}{\prod_{k=2}^{3N-4}\nu_k^{*}}\exp\left(-\frac{H_{\mathrm{kp}}(\tau_{yz})}{kT}\right) \qquad (1)$$

The first term of the pre-exponential factor in equation (1), $L\sqrt{2\pi m/kT}$, arises from the Goldstone mode because the stresses applied here are above the secondary Peierls stress, resulting in free kink motion along the dislocation line (L is the dislocation length and m is the atomic mass). The second term, $\prod_{i=1}^{3N-3}\nu_i^{\mathrm{init}}/\prod_{k=2}^{3N-4}\nu_k^{*}$,

[1]CEA, DEN, Service de Recherches de Métallurgie Physique, Gif-sur-Yvette 91191, France, [2]Laboratoire de Science et Ingénierie des Matériaux et Procédés, Grenoble Institute of Technology, CNRS, UJF, Saint Martin d'Hères 38402, France. *e-mail: David.Rodney@grenoble-inp.fr.

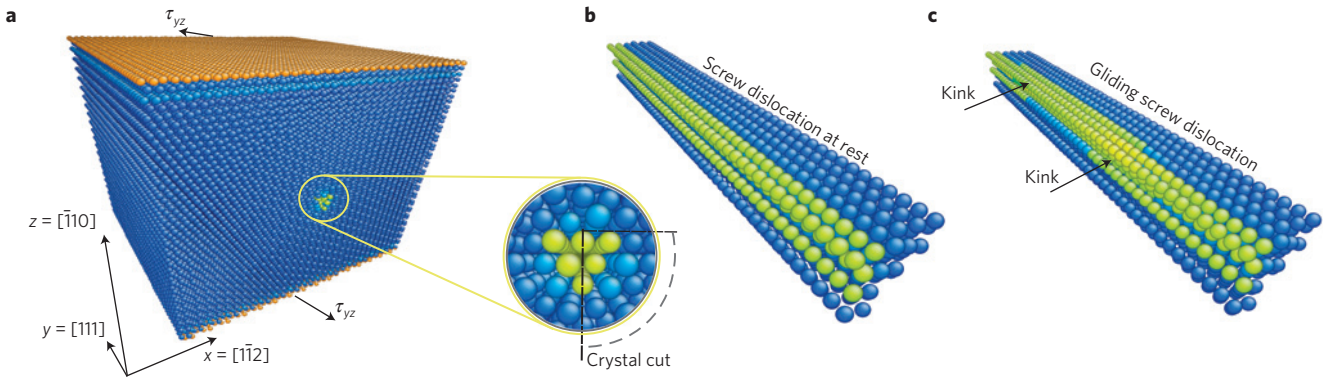

Figure 1 | Peierls mechanism of dislocation glide. A bcc iron crystal containing a screw dislocation is modelled with the interatomic potential proposed in ref. 20. **a**, Simulation cell. Atoms are coloured according to their potential energy and a τ_{yz} shear stress is applied to the free surfaces[14] (orange atoms). A crystal cut-through allows visualization of the atoms near the dislocation core (green–yellow atoms). **b**, Straight dislocation at rest. **c**, The dislocation glides through the nucleation and subsequent expansion of a kink pair.

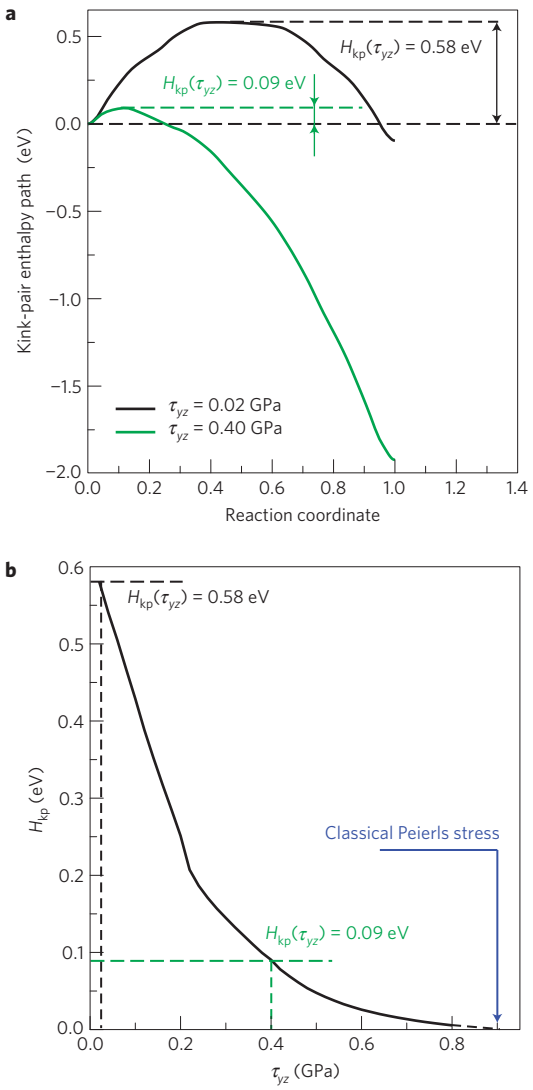

Figure 2 | Kink-pair enthalpy. a, Classical kink-pair minimum enthalpy path of a screw dislocation in iron, obtained at two different applied stresses using the nudged elastic band method[22]. **b**, Variation of the kink-pair formation enthalpy, the maximum enthalpy along the minimum enthalpy path, as a function of applied stress.

is the ratio of the partition functions of the harmonic vibrational modes of the crystal with real non-zero frequencies, $\{\nu_k^*\}$ and $\{\nu_i^{\text{init}}\}$, computed in the activated and initial states respectively, by diagonalizing the Hessian matrix of the system (see Methods).

It was shown[5] that quantum effects can be estimated within a harmonic TST by treating the vibrational modes quantum mechanically. Zero-point vibrations are included by replacing the classical oscillator partition functions by their quantum analogues and thermally assisted tunnelling near the top of the energy barrier is introduced by means of the transmission factor through the parabolic barrier associated with the unstable mode of the saddle configuration, of imaginary frequency $i\nu_{\text{US}}^*$. The resulting expression is (see ref. 24 and Supplementary Information for details):

$$\Gamma_{\text{quantum}} = L\sqrt{\frac{2\pi m}{kT}}\frac{h\nu_{\text{US}}^*/2kT}{\sin\left(h\nu_{\text{US}}^*/2kT\right)}\left(\frac{kT}{h}\right)^2 \times \frac{\prod_{i=1}^{3N-3}2\sinh\left(h\nu_i^{\text{init}}/2kT\right)}{\prod_{k=2}^{3N-4}2\sinh\left(h\nu_k^*/2kT\right)}\exp\left(-\frac{H_{\text{kp}}\left(\tau_{yz}\right)}{kT}\right) \quad (2)$$

The second term in the above expression, the transmission factor, diverges at a crossover temperature $T_{\text{tun}} = h\nu_{\text{US}}^*/2\pi k$, below which is the athermal deep tunnelling regime where the above approximation breaks down[24]. In the present calculations, T_{tun} lies between 1 and 6 K depending on the applied stress, thus limiting deep tunnelling to very low temperatures. Above T_{tun}, the transmission factor is close to unity and may be discarded in equation (2). In this regime, the quantum rate can be rewritten as a correction, δE, to the classical rate, known as Wigner correction[6]:

$$\Gamma_{\text{quantum}} = \exp\left(\frac{\delta E}{kT}\right)\Gamma_{\text{classic}} \quad \text{with}$$
$$\delta E = kT\ln\left(\frac{\prod_{i=1}^{3N-3}2\sinh\left(h\nu_i^{\text{init}}/2kT\right)/\left(h\nu_i^{\text{init}}/kT\right)}{\prod_{k=2}^{3N-4}2\sinh\left(h\nu_k^*/2kT\right)/\left(h\nu_k^*/kT\right)}\right) \quad (3)$$

As illustrated in Fig. 3a, Wigner correction deviates from zero over a wide temperature range. The transition temperature between quantum and classical regimes is half the Debye temperature, above which all hyperbolic sine functions in equation (3) can be replaced by their arguments. In this high-temperature regime where most experiments are performed, the present calculations are thus fully consistent with the classical TST of equation (1). In the low-

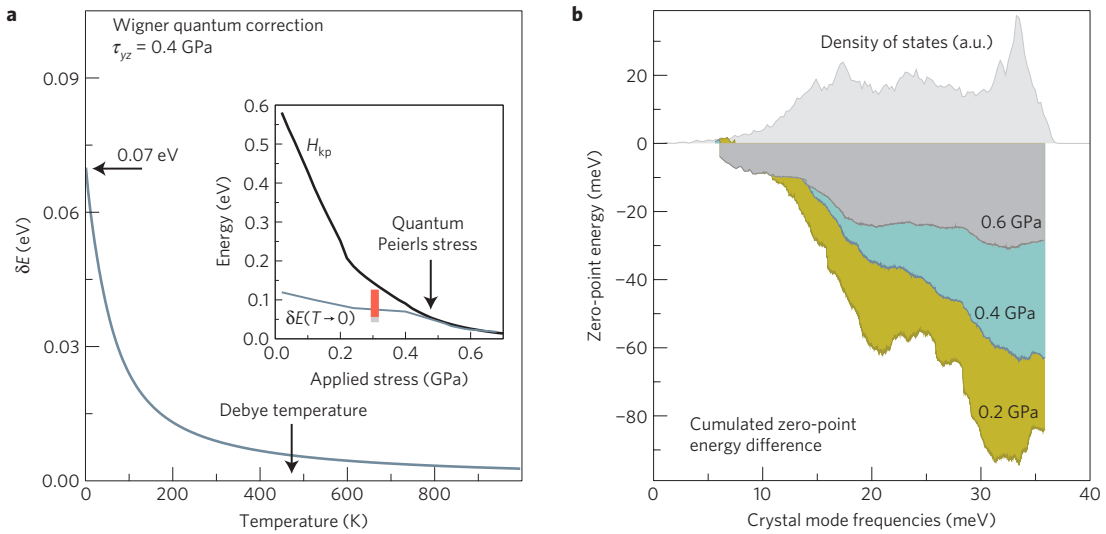

Figure 3 | Quantum effects on kink-pair formation. a, Temperature variation for the quantum correction δE at an applied stress of 0.4 GPa. In the inset, variation of the kink-pair formation enthalpy and correction term in the zero-temperature limit as a function of applied stress. **b**, Cumulated zero-point energy difference between the vibrational modes of the crystal with a dislocation containing a kink pair in the transition state and the crystal with a straight dislocation in equilibrium, against mode frequency. The phonon density of states with the same iron model is also reported.

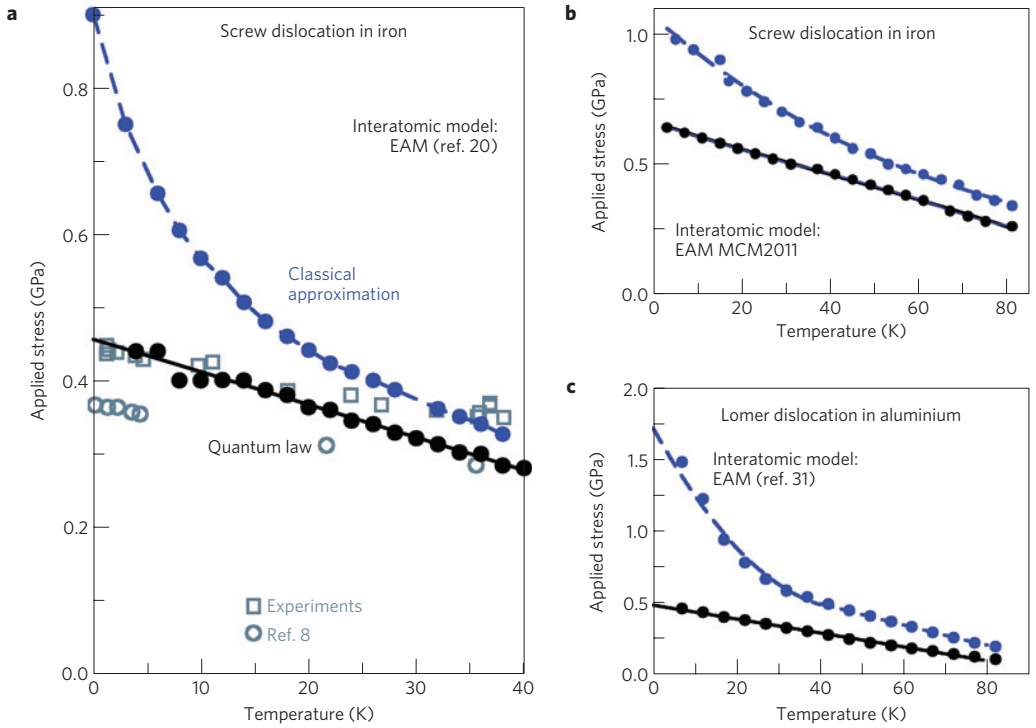

Figure 4 | Quantum Orowan law. a, Comparison of the temperature dependence of the applied stress predicted by the quantum Orowan law (solid curve), its classical approximation (dashed curve) and experimental data obtained with two crystal orientations in iron (open symbols)[8]. **b**, The same computations as in **a** with a different energetic model of iron, MCM2011 (see Supplementary Information). **c**, The same computations as in **a** for a different system, an $a/2\langle 110\rangle\{001\}$ edge Lomer dislocation in fcc aluminium[14].

temperature limit, the correction converges to the commonly used zero-point energy correction[6,25] $\sum_{i=1}^{3N-3} h\nu_i^{\text{init}}/2 - \sum_{k=2}^{3N-4} h\nu_k^*/2$. As shown in the inset of Fig. 3a, this limit increases with decreasing stress and is of the order of 0.1 eV, a significant fraction of the enthalpy H_{kp}. Corrections of the same order have been obtained for other processes, for instance surface adsorption[6] and diffusion[25]. As a result and as shown in the inset of Fig. 3a, the effective enthalpy H–δE becomes zero with the present iron model at an applied stress, which defines the quantum Peierls stress, close to 0.4 GPa. This stress is roughly half the classical Peierls stress, 0.9 GPa (Fig. 2b), in good agreement with the experimental value. To identify the physical origin of the quantum correction, we analysed the contribution of the different vibrational modes to the zero-point energy difference. We found that the main contribution comes from modes localized near the dislocation core. Typically, 90% of the correction is recovered when considering partial Hessian matrices restricted to the atoms within 0.7 nm of the dislocation core. However,

it seems from Fig. 3b that the quantum correction cannot be attributed to specific modes among those localized modes. Instead, the total cumulated zero-point energy difference arises from small modifications of many modes perturbed by the presence of the kink pair, with frequencies spreading over the entire phonon spectrum indicated by the density of state of the full crystal reported in Fig. 3b.

To compare with experiments at finite temperature, the plastic strain rate $\dot{\varepsilon}$ may be computed from the dislocation velocity using the Orowan equation[7], $\dot{\varepsilon} = \rho b v = \rho b a \Gamma$, where ρ is the dislocation density and b is the dislocation Burgers vector. Using the experimental value[8] for the strain rate ($\dot{\varepsilon} = 8 \times 10^{-5}\,s^{-1}$) and a dislocation density of $\rho = 10^{10}\,m^{-2}$ (this parameter has little influence and can be increased to $10^{12}\,m^{-2}$ without noticeable effect), the above relation can be inverted numerically to obtain the flow stress as a function of temperature, using either the quantum rate (equation (2)) or its classical approximation (equation (1)). Results are shown in Fig. 4a. In the zero-temperature limit, the quantum law tends to the quantum Peierls stress (Fig. 3a inset) whereas the classical approximation tends to the classical Peierls stress (Fig. 2b). The deviation between the quantum and classical laws decreases gradually over a broad range of temperatures, consistent with the quantum correction shown in Fig. 3a. Figure 4a compares our results with experimental data[8]. The agreement is particularly good with the present potential. To check the dependence of the correction on the energetic model, we developed a new interatomic potential, which predicts more accurately the screw dislocation Peierls potential (see Supplementary Information). The result is shown in Fig. 4b, confirming the large quantum correction at low temperatures. The new Peierls stress is 0.2 GPa above the experimental data. Such variability is expected among semi-empirical interatomic potentials, but it should be noted that the difference remains smaller than the 0.4 GPa decrease predicted with both potentials between classical and quantum Peierls stresses. Therefore, the quantum correction may not account for the entire discrepancy between simulations and experiments, but provides at least a large contribution. Note also that for both potentials, the flow stress with quantum correction decreases linearly with increasing temperature, in agreement with experimental data and in contrast with the classical law. To confirm the generality of the quantum effect discussed here and show that it is not limited to iron nor to bcc screw dislocations, the same effect is confirmed in Fig. 4c for a Lomer dislocation in a fcc crystal of aluminium (Fig. 4c). This dislocation is a non-conventional $a/2\langle 110\rangle\{001\}$ edge dislocation whose high Peierls stress is partly responsible for the strength of Lomer–Cottrell dislocation junctions[14].

The discrepancy between experimental and simulated Peierls stresses arises mainly from the quantum statistics of the crystal vibrational modes. Further theoretical improvements should include electronic structure methods, based on the density functional theory[12,21] or for instance bond order potentials[26] to reduce uncertainties related to the interatomic potential. The present work shows the importance of accounting for quantum effects when simulating crystal plasticity at low temperature and may also provide a theoretical basis for interpreting recent *in situ* observations of a low-temperature jerky dislocation glide regime[17]. Other plasticity processes should be revisited, including dislocation glide in covalent crystals[27], solid solutions[28] and dislocation nucleation from thermally activated sources, where vibrations also play an important role[29]. Finally, the quantum correction used here applies in principle to all thermally activated processes and is expected to be significant if the energy barrier is small enough that the corresponding kinetics remains measurable experimentally at low temperatures. In this context, vacancy migration[30] is another process worth investigating in detail.

Methods

Classical kink-pair formation. The simulation cell has bcc symmetry with 20, 54 and 22.5 repeating units in directions x[211], y[111] and z[011], respectively ($N = 123,120$ atoms). Periodic boundary conditions are applied in directions x and y (with fixed cell dimensions) whereas the z surfaces are free. A screw dislocation with Burgers vector $b = a/2$[111] is introduced along the central [111] axis of the cell by means of its elastic displacement field, followed by energy minimization. A shear stress τ_{yz} is applied on the {011}[111] slip system by adding external forces to the atoms in the upper and lower z surfaces[14].

The minimum enthalpy path between successive equilibrium configurations of the dislocation in direction x is computed using the climbing nudged elastic band method[14,22] with an improved tangent calculation to minimize the total energy of a chain of 90 crystal replicas linked by harmonic springs of strength 10 eV Å^{-1}. We further asserted the validity of the transition states by checking that they were first-order saddle points (with a force of less than 10^{-2} eV nm^{-1} and a single negative eigenvalue) and checking their connectivity to the initial and final states by re-relaxations following forward and backward perturbations along the eigenvector of the imaginary mode.

Harmonic vibrational frequencies. Normal-mode frequencies in equations (1)–(3) are computed by diagonalizing the Hessian matrix of the initial equilibrium and activated states of the dislocation at each applied stress. Exact diagonalizations were performed using ScaLAPACK parallel routines on 2,304 central processing units. We checked that the correction in equation (3) does not depend appreciably on cell dimensions in the range accessible to our computational capabilities.

Received 1 May 2012; accepted 13 July 2012; published online 12 August 2012

References

1. Peierls, R. E. On the size of a dislocation. *Proc. Phys. Soc. Lond.* **52,** 34–37 (1940).
2. Basinski, Z. S., Duesbery, M. S. & Taylor, R. Influence of shear stress on screw dislocations in a model sodium lattice. *Can. J. Phys.* **49,** 2160–2180 (1971).
3. Suzuki, H. in *Fundamental Aspects of Dislocation Theory* (eds Simmons, J. A., de Wit, R. & Bullough, R.) 253–272 (Spec. Publ. 317, Nat. Bur. Stand., 1970).
4. Takeuchi, S., Hashimoto, T. & Maeda, K. Plastic deformation of bcc metal single crystals at very low temperatures. *Trans. Jpn Inst. Met.* **23,** 60–69 (1982).
5. Wigner, E. The transition state method. *Trans. Faraday Soc.* **34,** 29–41 (1938).
6. Henkelman, G., Arnaldsson, A. & Jónsson, H. Theoretical calculations of CH_4 and H_2 associative desorption from Ni(111): Could subsurface hydrogen play an important role? *J. Chem. Phys.* **124,** 044706 (2006).
7. Orowan, E. Problems of plastic gliding. *Proc. Phys. Soc.* **52,** 8–22 (1940).
8. Kuramoto, E., Aono, Y., Kitajima, K., Maeda, K. & Takeuchi, S. Thermally activated slip deformation between 0.7 and 77 K in high-purity iron single crystals. *Phil. Mag. A* **39,** 717–724 (1979).
9. Brunner, D. & Diehl, J. Extension of measurements of the tensile flow stress of high-purity α-iron single crystals to very low temperatures. *Z. Metalkd.* **83,** 828–834 (1992).
10. Marian, J., Cai, W. & Bulatov, V. V. Dynamic transitions from smooth to rough to twinning in dislocation motion. *Nature Mater.* **3,** 158–163 (2004).
11. Chaussidon, J., Fivel, M. & Rodney, D. The glide of screw dislocations in bcc Fe: Molecular statics and dynamics simulations. *Acta Mater.* **54,** 3407–3416 (2006).
12. Woodward, C. & Rao, S. I. Flexible *ab initio* boundary conditions: Simulating isolated dislocations in bcc Mo and Ta. *Phys. Rev. Lett.* **88,** 216402 (2002).
13. Li, J. *et al.* Core energy and Peierls stress of a screw dislocation in bcc molybdenum: A period-cell tight-binding study. *Phys. Rev. B* **70,** 104113 (2004).
14. Rodney, D. & Proville, L. Stress-dependent Peierls potential: Influence on kink-pair activation. *Phys. Rev. B* **79,** 094108 (2009).
15. Gröger, R. & Vitek, V. Explanation of the discrepancy between the measured and atomistically calculated yield stress in body-centered cubic metals. *Phil. Mag. Lett.* **87,** 113–120 (2007).
16. Bulatov, V. V. & Cai, W. Nodal effects in dislocation mobility. *Phys. Rev. Lett.* **89,** 115501 (2002).
17. Caillard, D. Kinetics of dislocations in pure Fe. Part II. In situ straining experiments at low temperature. *Acta Mater.* **58,** 3504–3515 (2010).
18. Gilman, J. J. Escape of dislocations from bound states by tunneling. *J. Appl. Phys.* **39,** 6086–6090 (1968).
19. Indenbom, V. L., Petukhov, B. V. & Lothe, J. in *Elastic Strain Fields and Dislocation Mobility* (eds Indenbom, V. L. & Lothe, J.) 489–516 (Elsevier, 1992).
20. Gordon, P. A., Neeraj, T. & Mendelev, M. I. Screw dislocation mobility in BCC Metals: A refined potential description for α-Fe. *Phil. Mag. Lett.* **91,** 3931–3945 (2011).

21. Ventelon, L. & Willaime, F. Core structure and Peierls potential of screw dislocations in α-Fe from first principles: Cluster versus dipole approaches. *J. Computer-aided Mater. Des.* **14,** 85–94 (2007).
22. Henkelman, G., Uberuaga, B. P. & Jónsson, H. A climbing image nudged elastic band method for finding saddle points and minimum energy paths. *J. Chem. Phys.* **113,** 9901–9904 (2000).
23. Vineyard, G. H. Frequency factors and isotope effects in solid state rate processes. *J. Phys. Chem. Solids* **3,** 121–127 (1957).
24. Benderskii, V. A., Makarov, D. E. & Wight, C. A. *Chemical Dynamics at Low Temperature* (Wiley, 1994).
25. Johnson, D. F. & Carter, E. A. Hydrogen in tungsten: Absorption, diffusion, vacancy trapping, and decohesion. *J. Mater. Res.* **25,** 315–327 (2010).
26. Mrovec, M., Nguyen-Manh, D., Elsässer, C. & Gumbsch, P. Magnetic bond-order potential for iron. *Phys. Rev. Lett.* **106,** 246402 (2011).
27. Pizzagalli, L. & Beauchamp, P. First principles determination of the Peierls stress of the shuffle screw dislocation in silicon. *Phil. Mag. Lett.* **84,** 729–736 (2004).
28. Curtin, W. A., Olmsted, D. L. & Hector, L. G. A predictive mechanism for dynamic strain ageing in aluminum–magnesium alloys. *Nature Mater.* **5,** 875–880 (2006).
29. Ryu, S., Kang, K. & Cai, W. Entropic effect on the rate of dislocation nucleation. *Proc. Natl Acad. Sci. USA* **108,** 5174–5178 (2011).
30. Derlet, P. M., Nguyen-Manh, D. & Dudarev, S. L. Multiscale modeling of crowdion and vacancy defects in body-centered cubic transition metals. *Phys. Rev. B* **76,** 054107 (2007).
31. Ercolessi, F. & Adams, J. Interatomic potentials from first-principles calculations: The force-matching method. *Europhys. Lett.* **26,** 583–588 (1994).

Acknowledgements

This work was performed using HPC resources from GENCI-[CCRT/CINES] (Grant 2012096973). D.R. was supported by the Institut Universitaire de France.

Author contributions

All authors contributed equally to the present work.

Additional information

Supplementary information is available in the online version of the paper. Reprints and permissions information is available online at www.nature.com/reprints. Correspondence and requests for materials should be addressed to D.R.

Competing financial interests

The authors declare no competing financial interests.

the HOMO is located around −5 to −6 eV versus vacuum, whereas the LUMO ranges from about −2 to −3 eV. As illustrated in Fig. 1, defects or impurities frequently have empty orbitals below −3 eV that can take up an electron. Filled orbitals above −5 eV (suitable for accepting holes) are more elusive. The way to obtain similar mobilities for electrons and holes is hence clear: eliminate the electron traps.

A beautiful example of this approach was reported by Chua and co-workers for OFETs (ref. 4). They found that electronegative hydroxyl groups at the interfaces between organic semiconductors and gate dielectrics are responsible for electron trapping. When they used dielectric materials that were free of hydroxyl groups, electron transport was uninhibited and n-type transistors could be realized, even with materials that were originally thought to be p-type semiconductors. This opened the way to ambipolar and light-emitting transistors. The Blom group[1,3] applied this principle to semiconducting polymers used in OLEDs and OSCs, where charge transport proceeds through the bulk of the semiconductor film.

In 2010, Zhang and co-workers validated that the electron and hole mobility were indeed equal for the prototypical semiconducting polymer (poly(2-methoxy-5-(2′-ethylhexyloxy)-1,4-phenylenevinylene) when the electron traps were filled up by doping[3]. The present work from Nicolai and colleagues now shows that this approach may be generalized and applied to a wide range of semiconducting polymers[1]. Their results also explain the paradox that electron and hole mobility appear equal in microwave conductivity measurements[5], but not in measurements with other, macroscopic techniques[6]. When the conductivity is measured by analysing the absorption of microwave radiation, charges are accelerated and decelerated by the electromagnetic field only over a short section of a polymer chain where trapping effects do not take place, in contrast to the macroscopic transport over many chains.

The result by Nicolai and co-workers is a major advance in two ways. For those interested in the application of organic semiconductors, it can guide the design of p-type or n-type materials and the development of more efficient organic electronic devices. At the same time, their finding implies that ambipolar high-mobility materials for bulk film applications need to have small HOMO–LUMO gaps, as is the case for many solar-cell materials — for large gaps, either electrons or holes will be susceptible to trapping. To those interested in fundamental charge transfer processes in π-conjugated materials, these results provide a clear understanding of the limitations of electron transport. With this knowledge, a quantitative and unified description of the current flow in organic semiconductors has become possible. ❐

Anna Köhler is at the Department of Physics and at the Bayreuth Institute of Macromolecular Science, University of Bayreuth, 95440 Bayreuth, Germany.
e-mail: anna.koehler@uni-bayreuth.de

References

1. Nicolai, H. T. *et al. Nature Mater.* **11,** 882–887 (2012).
2. Warta, W., Strehle, R. & Karl, N. *Appl. Phys. A* **36,** 163–170 (1985).
3. Zhang, Y., De Boer, B. & Blom, P. W. M. *Phys. Rev. B* **81,** 085201 (2010).
4. Chua, L-L. *et al. Nature* **434,** 194–199 (2005).
5. Prins, P. *et al. Adv. Mater.* **17,** 718–273 (2005).
6. Bässler, H. & Köhler, A. *Top. Curr. Chem.* **312,** 1–66 (2012).

MECHANICAL PROPERTIES

Overcoming old barriers

Dislocation motion is crucial to the deformation of materials. The discovery that at least at lower temperatures quantum effects play an important role in this process considerably improves quantitative predictions of mechanical properties.

G. J. Ackland

When metals such as iron and steel deform, they do so via the movement of dislocations through the crystal. These long, one-dimensional line defects don't move easily, which is the reason why iron can be hard to deform. The stress required to overcome this resistance to motion, the so-called Peierls stress, depends on the crystal structure. In face-centred cubic (fcc) materials it generally is low, increasing with temperature, whereas in body-centred cubic (bcc) materials it is higher, but thermal fluctuations have a stronger influence so that the Peierls stress drops as temperature rises.

It is believed that the rate-limiting step is the nucleation of a kink-pair: two steps on the dislocation line, which once created move easily along the line moving it forwards. However, there has been a longstanding discrepancy between theory and experiment regarding the behaviour of dislocations at low temperatures in iron and other bcc metals. Across a range of materials, calculations based on the classical transition-state theory applied to kink-pair creation, generally overestimate the energetic barrier involved. Many explanations have been put forward to explain the reduced barriers seen in experiments. Defects for example might assist the nucleation. Writing in *Nature Materials*, Laurent Proville and colleagues have now performed calculations on dislocation movements in iron that suggest that the classical transition-state theory itself is at fault: quantum effects must be invoked to describe the system[1].

Transition-state theory has been such a central part of understanding reaction rates that its fundamental tenets typically go unchallenged. In an approach first formulated by Eugene Wigner[2], to transit from one macrostate to another required the free-energy barrier to be defined: we must consider a thermally averaged 'transition state'. This state corresponds to the barrier, and is treated as a macrostate distinguished from the initial and final states. Practically, it may seem odd that modes with frequencies much lower than the time corresponding to the barrier crossing should be included in the calculation, because how can some vibration that doesn't have time to happen enter into the calculation? However, in the classical case it turns out to be fine, but in a quantum picture this is more troublesome (Fig. 1).

In the classical case such approximations are appropriate, because transition-state theory is usually applied to chemical reactions at high temperatures and reaction rates at low temperatures are negligible. In direct molecular dynamics simulations, the atoms are therefore treated classically and quantum effects such as tunnelling and

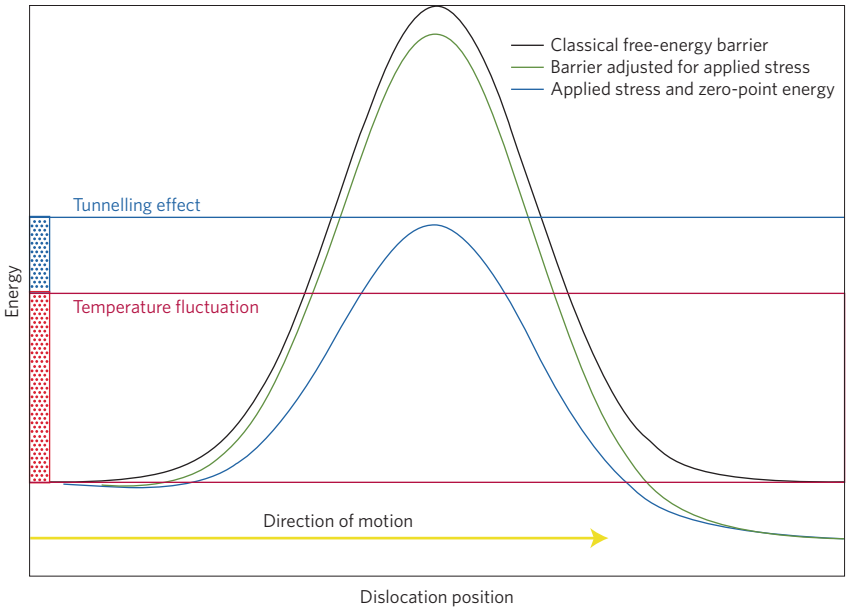

Figure 1 | Overcoming activation barriers. There is a formidable energetic barrier for dislocation nucleation and motion (black curve). This barrier can be lowered by applied stress (green curve; the Peierls stress would remove it altogether). In a quantum mechanical treatment, zero-point motion lowers the barrier still further (blue curve). Moreover, temperature fluctuations allow the dislocation to jump over the barrier, and quantum tunnelling allows it to pass through.

zero-point energy are neglected. Materials scientists have adopted this standard approach, even though the full quantum treatment is well known and despite the fact that even at lower temperatures dislocation motion can still occur because it is induced both by stress and temperature, so motion still is induced at high enough stress.

Quantum effects that play a role in transition-state theory at lower temperatures include zero-point motion and tunnelling across the barrier. Zero-point motion describes the effect where even in the ground state random thermal fluctuations cause the energy of a system to increase and thereby assist in overcoming transition barriers. As for quantum mechanical tunnelling through the barrier, Proville and colleagues have shown that this effect is relevant only at extremely low temperatures, much below the experimental discrepancy. The effect of quantum statistics and zero-point motion, however, is important up to about half the Debye temperature, which describes the temperature above which classical statistics are valid. As Proville and colleagues find, these zero-point motions approximately halve the Peierls stress for dislocation motions in the low-temperature limit — in good agreement with experiment.

To reach this conclusion, the researchers consider strain fields around dislocations, which are a significant contribution to the behaviour of dislocations, and their accurate modelling depends critically on the empirical potential used to describe these fields. Here, two models were tested, each reproduces reasonably well the transition barrier and vibration properties calculated with more accurate quantum mechanical schemes. Each gives similar results. The computational efforts cannot be underestimated, and would have been impossible a few years ago. Even with these simple force models, the calculations require diagonalization of matrices with over ten billion elements. When analysing all phonon modes to the dislocation movement, it turns out that there are no particular vibrations responsible for lowering the activation barrier. Rather, the activated state is associated with a softening of all modes near to the dislocation core. In classical theory, these modes do not contribute at low temperature, however, in a quantum treatment they lower the barrier due to its reduced zero-point energy.

The iron calculation is backed by a similar work on another high Peierls stress configuration, a Lomer–Cottrell dislocation in Al. Again, a softening of the modes around the activated state reduced the stress required to move the defect at low temperatures. This provides further evidence that quantum effects should be included in transition rate, and that after 75 years, Wigner's work still needs to be read. ❐

G. J. Ackland is at the University of Edinburgh, School of Physics and Astronomy, Mayfield Road, Edinburgh EH9 3JZ, UK.
e-mail: gjackland@ed.ac.uk

References

1. Proville, L., Rodney, D. & Marinica, M-C. **11,** 845–849 (2012).
2. Wigner, E. *Trans. Faraday Soc.* **34,** 29–41 (1938).

CRYSTAL NUCLEATION

Nucleus in a droplet

Real-time transmission electron microscopy shows that the formation of crystal nuclei of organic molecules in solution occurs inside dense liquid nanoclusters.

Peter G. Vekilov

It is common experience that the evaporation of carbon dioxide in a freshly poured glass of a carbonated soft drink proceeds slowly through the formation of discrete bubbles at a few spots on the glass. This is because the formation of the new phase (gas) from the old phase (supersaturated liquid) is hindered by the free-energy penalty associated with the creation of the interface separating the two phases. This free-energy barrier — which determines the rate at which the new phase forms — is lowered when a nucleus of the new phase forms on a foreign surface of proper composition and configuration

Supplementary notes to: Quantum effect on thermally activated glide of dislocations

L. Proville[(1)], D. Rodney[(2)] and M.C. Marinica[(1)]
(1) CEA, DEN, Service de Recherches de Métallurgie Physique, 91191 Gif-sur-Yvette, France and
(2)Laboratoire de Science et Ingénierie des Matériaux et Procédés (SIMAP-GPM2),
Grenoble Institute of Technology, Saint Martin d'Hères 38402, France

Supplementary information is provided regarding (i) the quantum transition state theory used to predict dislocation kinetics, and (ii) a new interatomic potentials employed to model screw dislocations in body centered cubic iron.

I. DERIVATION OF QUANTUM OROWAN LAW

To study the influence of quantum effects in dislocation glide, we employ a quantum harmonic approximation of the transition state theory (TST) (see Ref. [1] in Supplementary bibliography), the basic ingredients of which are presented hereafter. We consider a b.c.c. crystal where plasticity is thermally-activated and controlled by the formation of kink pairs on screw dislocations. The plastic strain rate is given by Orowan law:

$$\dot{\epsilon} = \rho_d b V_d \tag{1}$$

where ρ_d is the density of mobile screw dislocations, b the Burgers vector and V_d the average screw dislocation velocity. Dislocation glide being controlled by the formation of kink pairs between nearest Peierls valleys, the dislocation velocity is expressed as $V_d = a\Gamma$ where a is the distance between Peierls valleys and Γ the kink-pair nucleation rate. According to the classical TST (see [2] in Supplementary bibliography), the rate Γ for a three-dimensional system made of N atoms of equal mass m is expressed as an integral over phase space:

$$\Gamma = Z_r^{-1} \int \prod_{i=1}^{3N} \frac{dX_i dP_i}{h^{3N}} \delta(\mathbf{X} - \mathbf{X_s}) \frac{|\mathbf{P}.\mathbf{d}_s|}{m} \theta(\mathbf{P}.\mathbf{d}_s) \exp\left[-\beta \mathcal{H}(\mathbf{P}, \mathbf{X})\right], \tag{2}$$

where thick symbols stand for 3N-dimensional vectors. $\mathbf{X}_s$ is the transition state, i.e. the unstable dislocation configuration between Peierls valleys, $\mathbf{d}_s$ is the corresponding unstable eigenmode, $\mathcal{H}(\mathbf{P}, \mathbf{X})$ the Hamiltonian of the system to which the work of applied stress is properly substrated, and Z_r is the reactant partition function, the harmonic partition function of the crystal with a screw dislocation lying at the bottom in its Peierls valley. The three free translational modes of the system have no contribution to the rate Γ since they equally contribute to Z_r and to the numerator in Eq. 2. They are omitted in the following.

To introduce the harmonic approximation, we use a normal mode representation $(\mathbf{q}, \mathbf{p})$ computed at the saddle state, instead of the coordinates $(\mathbf{X}, \mathbf{P})$. The unstable mode is placed at the end of the mode list, i.e. $s = 3N - 3$. If we note λ_ν the eigenvalue of mode ν, the kink-pair nucleation rate is then written as:

$$\Gamma = {Z_r}^{-1} \int \frac{dq_s dp_s}{h} \frac{p_s}{m} \theta(p_s) \delta(q_s) \prod_{\nu=1}^{3N-4} \frac{dq_\nu dp_\nu}{h^{3N-4}} \exp\left[-\beta \left(H_{kp} + \sum_{\nu=1}^{3N-3} [\frac{p_\nu^2}{2m} + \lambda_\nu \frac{q_\nu^2}{2}] \right)\right], \tag{3}$$

where H_{kp} is the activation enthalpy for kink-pair formation (the enthalpy difference between saddle and initial states), function of the applied shear stress τ_{yz}.

In b.c.c crystals, the secondary Peierls stress, that is the Peierls stress for kink motion along the screw dislocation line, is small (a few MPa) compared to the primary Peierls stress. As a result, in the stress regime considered here, there is no resistance for kink motion along the dislocation line, resulting in a Goldstone mode of zero eigenvalue. The latter, assumed to correspond to $\nu = 1$, can be integrated out (it corresponds to the Gaussian integration of a kinetic energy term $1/h \int dq dp \exp(-\beta p^2/2m) = L\sqrt{2\pi mkT}/h$), yielding:

$$\Gamma = \frac{L\sqrt{2\pi mkT}}{hZ_r} \int \frac{dq_s dp_s}{h} \frac{p_s}{m} \theta(p_s) \delta(q_s) \prod_{\nu=2}^{3N-4} \frac{dq_\nu dp_\nu}{h^{3N-5}} \exp\left[-\beta \left(H_{kp} + \sum_{\nu=2}^{3N-3} [\frac{p_\nu^2}{2m} + \lambda_\nu \frac{q_\nu^2}{2}] \right)\right]. \tag{4}$$

Note that the dislocation length L now appears explicitly in the nucleation rate, a result of the integration of the Goldstone mode.

At low temperature, quantum mechanics must be accounted for. Since the normal modes are independent of one another, each stable mode (for $\nu = 2$ to $3N-4$) yields in Eq. 4 the partition function of a quantum harmonic oscillator $[2\sinh(\frac{\hbar\beta}{2}\omega_\nu)]^{-1}$, where $\omega_\nu = \sqrt{\lambda_\nu/m}$ is the angular frequency of mode ν. Similarly, the partition function in the stable reactant state Z_r can be treated harmonically, yielding $Z_r = \prod_{\mu=1}^{3N-3} [2\sinh(\frac{\hbar\beta}{2}\Omega_\mu)]^{-1}$, with $\{\Omega_\mu\}$ the angular frequencies associated with the reactant state. This gives

$$\Gamma = \frac{L\sqrt{2\pi mkT} \prod_{\mu=1}^{3N-3} [2\sinh(\frac{\hbar\beta}{2}\Omega_\mu)]}{h \prod_{\nu=2}^{3N-4} [2\sinh(\frac{\hbar\beta}{2}\omega_\nu)]} I, \tag{5}$$

where the integral I is defined by:

$$I = \int \frac{dq_s dp_s}{h} \frac{p_s}{m} \theta(p_s) \delta(q_s) \exp\left[-\beta \left(\frac{p_s^2}{2m} + H_{kp} + \lambda_s \frac{q_s^2}{2} \right)\right]. \tag{6}$$

This integral over coordinate q_s of the unstable mode can be replaced (Ref. [1] in Supplementary bibliography) by the crossing rate of the parabolic barrier $H_{kp} + \lambda_s \frac{q_s^2}{2}$ which leads to

$$I = \frac{1}{h} \int dE\ W(E) \exp\left(-\beta E\right), \tag{7}$$

where W, the transmission coefficient for a parabolic barrier (Ref. [3] in Supplementary bibliography), is given by $W(E) = [1 + \exp\left(2\pi(H_{kp} - E)/\hbar\omega_s\right)]^{-1}$ and $\omega_s = \sqrt{-\lambda_s/m}$. After simplication, the integral becomes:

$$I = \frac{kT}{h} \frac{\hbar\beta\omega_s/2}{\sin\left(\hbar\beta\omega_s/2\right)} e^{-\beta H_{kp}}. \tag{8}$$

Within the present harmonic TST, the rate of kink pair formation is:

$$\Gamma = L\sqrt{\frac{2\pi m}{kT}} \frac{\hbar\beta\omega_s/2}{\sin\left(\hbar\beta\omega_s/2\right)} \left(\frac{kT}{h}\right)^2 \frac{\prod_{\mu=1}^{3N-3}[2\sinh(\frac{\hbar\beta}{2}\Omega_\mu)]}{\prod_{\nu=2}^{3N-4}[2\sinh(\frac{\hbar\beta}{2}\omega_\nu)]} e^{-\beta H_{kp}}, \tag{9}$$

which corresponds to Eq. 2 in the main text, replacing the circular frequencies ω's with frequencies ν's and accordingly $\hbar$ with h. Combining this equation with Eq. 1, we can therfore express the plastic strain rate as a quantum thermally-activated Orowan law. In experimental conditions of plastic deformation, $\dot{\epsilon}$ is constant, and so are a, b and ρ_d approximately. Eq. 1 then becomes a self-consistent equation between the applied stress τ_{yz} (which sets the saddle state and thus sets H_{kp}, ω_s, $\{\omega_\nu\}$ and $\{\Omega_\mu\}$) and the temperature T. It is well-known (Ref. [4] and Ref. [1] in Supplementary bibliography) that Eq. 8 diverges at a critical temperature $T_{\rm tun} = \hbar\omega_s/2\pi k$, the temperature below which the deep quantum tunneling can not be neglected. The above harmonic theory is thus valid only above $T_{\rm tun}$. Below, nonlinear effects must be accounted for, which is the subject of the instanton theory developed by Miller (Ref. [2] in Supplementary bibliography). The most important contribution of quantum mechanics comes from the crystal partition functions that appear in the pre-exponential factor in Eq. 9. This quantum correction has some similarities with the heat capacity deviation from the Dulong-Petit law (see textbooks as Ref. [5] in Supplementary bibliography).

II. INTERATOMIC POTENTIAL FOR SCREW DISLOCATIONS WITH REALISTIC PEIERLS BARRIER

The interatomic potentials employed in the present work are based on the Embedded Atom Method (EAM) (Ref. [6] in Supplementary bibliography) and require to adjust fitting parameters. Very few potentials can be used to model dislocations in bcc crystals because most potentials predict a screw dislocation core structure in disagreement with first-principles calculations. The most-widely used EAM potential, developed by Mendelev *et al.* (Ref. [7] in Supplementary bibliography) predicts the correct core structure but unfortunately predicts also an intermediate metastable dislocation configuration, which is not confirmed by first-principles calculations, as can be seen in the Peierls potentials reported in Supplementary Fig. 1. In the main article, we employed a very recent EAM potential developed by Gordon *et al.* (Ref. [20] in main text reported as Ref. [8] in Supplementary bibliography) , which predicts both the correct core structure and also only a very shallow intermediate position. This choice of potential also avoids any concern about the parameter adjustments, since the potential was not developed specifically to treat quantum effects. However, according to this potential, the Peierls barrier for the screw dislocation is 10 meV per burgers vector, while ab-initio calculations (Ref. [9] in Supplementary bibliography) yield a barrier of 27 meV/b.

In order to check whether the form and amplitude of the Peierls barrier affects the main result of our study, i.e. a reduction of the Peierls stress by quantum effects, we developed a new EAM parametrization to describe more accurately the $a/2\langle 110\rangle\{111\}$ screw dislocation. Our new potential, hereafter denoted by MCM2011, correctly reproduces the non-degenerate compact core structure of the screw dislocation, with a $\{110\}$ glide plane and a single hump Peierls potential, without intermediate metastable configuration (see Supplementary Fig. 1). Clearly, MCM2011 is in very satisfactory agreement with the ab-initio computations in iron, with a Peierls barrier of about 29 meV/b.

The functional form of MCM2011 is the same as in Ref. [7] in Supplementary bibliography. The energy is written

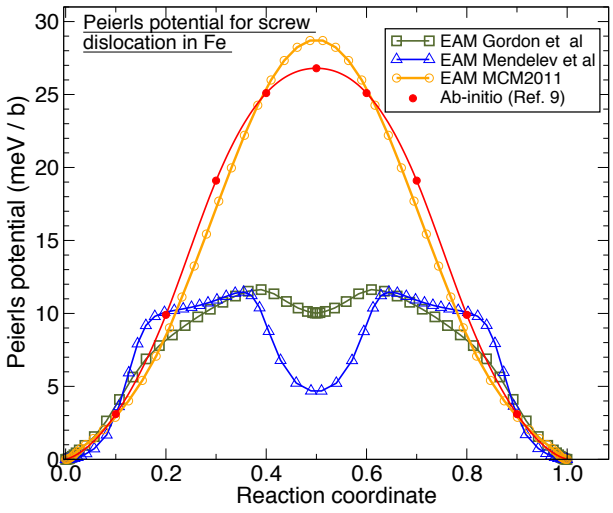

FIG. 1. The Peierls barrier for a straight screw dislocation in an α-Fe crystal without applied stress, computed with different Embedded Atom Method potentials and electronic-structure first-principles calculations (Ref. [9] in Supplementary bibliography) (see legend).

a_1^ϕ	(δ_1^ϕ)	-0.935107781301912E+01 (2.30)
a_2^ϕ	(δ_2^ϕ)	0.268772796931241E+02 (2.40)
a_3^ϕ	(δ_3^ϕ)	-0.517763908172230E+01 (2.50)
a_4^ϕ	(δ_4^ϕ)	0.921879058893854E+00 (2.60)
a_5^ϕ	(δ_5^ϕ)	0.912101025455097E+00 (2.80)
a_6^ϕ	(δ_6^ϕ)	0.381066389501505E+00 (3.00)
a_7^ϕ	(δ_7^ϕ)	0.355564566504528E+00 (3.60)
a_8^ϕ	(δ_8^ϕ)	-0.930892645563238E+00 (3.80)
a_9^ϕ	(δ_9^ϕ)	0.168191193670112E+01 (4.20)
a_{10}^ϕ	(δ_{10}^ϕ)	-0.906404101574372E+00 (4.40)
a_{11}^ϕ	(δ_{11}^ϕ)	0.978983139615580E-01 (4.60)
a_{12}^ϕ	(δ_{12}^ϕ)	-0.431620950508167E+00 (4.80)
a_{13}^ϕ	(δ_{13}^ϕ)	0.184733884152394E+00 (5.20)
a_1^ρ	(δ_1^ρ)	0.701512219990929E+01 (2.10)
a_2^ρ	(δ_2^ρ)	0.194060579359683E+02 (2.40)
a_3^ρ	(δ_3^ρ)	-0.213254828113481E+00 (3.20)
a_4^ρ	(δ_4^ρ)	0.256174912582562E+00 (4.20)
a_5^ρ	(δ_5^ρ)	0.152483050063800E-02 (5.00)
a_1^F		-1.0
a_2^F		-0.776551760170000D-04

TABLE I. Parameters describing MCM2011 EAM potential for iron with all distances expressed in Å and energies in eV. See Eqs. 10, 11, 12 and 13.

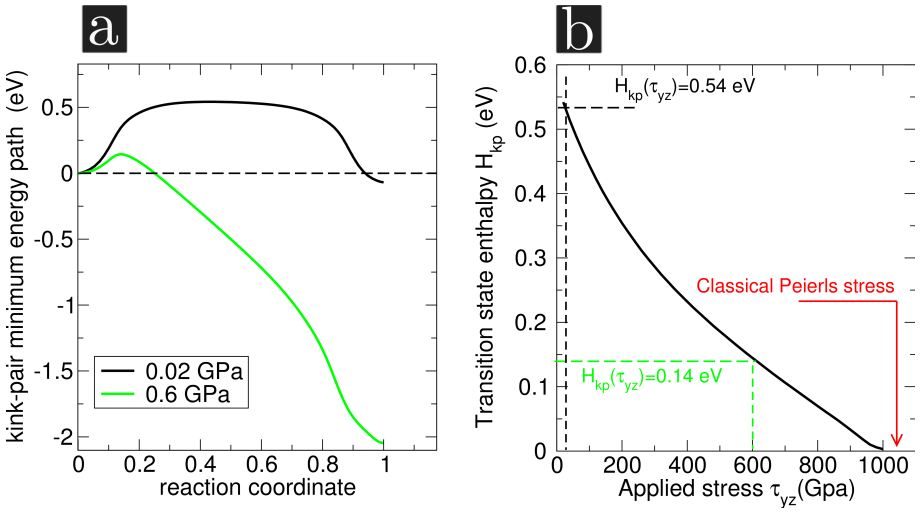

FIG. 2. (a) Kink-pair minimum enthalpy paths at two applied stresses (see legend) and (b) variation of the kink-pair formation enthalpy as a function of the applied stress. All curves were obtained using the MCM2011 EAM potential for bcc iron.

as:

$$V\left(\mathbf{r_1},\ldots,\mathbf{r_N}\right)=\sum_{i=1}^{N}\left[\frac{1}{2}\sum_{j\neq i}^{N}\phi(r_{ij})+F\left(\rho_i\right)\right] \tag{10}$$

$$\phi\left(x\right)=\sum_{i=1}^{n^{\phi}}a_i^{\phi}\left(\delta_i^{\phi}-x\right)^3\theta\left(\delta_i^{\phi}-x\right) \tag{11}$$

$$\rho\left(x\right)=\sum_{i=1}^{n^{\rho}}a_i^{\rho}\left(\delta_i^{\rho}-x\right)^3\theta\left(\delta_i^{\rho}-x\right) \tag{12}$$

$$F\left(x\right)=a_1^F\sqrt{x}+a_2^F x^2, \tag{13}$$

where θ stands for the Heaviside step function. The parameters of the potential are given in Table II. In addition to the screw dislocation Peierls barrier, various other physical quantities were adjusted in order to ensure transferability of the potential. The database contains three other components:

1. experimental values of solid state properties: lattice parameters and cohesive energies of the f.c.c./b.c.c. structures, elastic constants C_{11}, C_{12} and C_{44}

2. ab-initio formation energies of basic point defects: mono-interstitial with different orientations ($\langle 110\rangle$, $\langle 111\rangle$, $\langle 100\rangle$, octahetral and tetrahedral) and the mono-vacancy. These reference values were calculated using the SIESTA code in the DFT-GGA approximation,

3. ab-initio forces acting on atoms in liquid and random state configurations as in Ref. [7] in Supplementary bibliography.

More details about the physical properties obtained from MCM2011 will be the subject for a future publication.

Using MCM2011, the enthalpy H_{kp} for kink-pair formation was computed (see Fig. 2 (a) and (b)) in the same simulation cell as in the main article. With this new EAM, the classical Peierls stress is 1.05 GPa.

Because of the computational load involved in determining the crystal mode frequencies, calculations of the latter were performed in a simulation cell smaller than in the main article: the number of atoms is $N = 17\,136$, with 12, 34 and 10.5 repeating units in directions x$[\bar{2}11]$, y$[111]$ and z$[01\bar{1}]$.

According to Fig. 4 b, in the main text, the computation of the quantum Peierls stress with MCM2011 potential (0.65 GPa) overestimates the experimental Peierls stress and it is larger than the quantum Peierls stress obtained with Gordon's potential (0.45 GPa). Such variations are inherent to EAM potentials, to which we are compelled by the too large computational load required to first-principles capabilities. Fortunately, the departure in the EAM

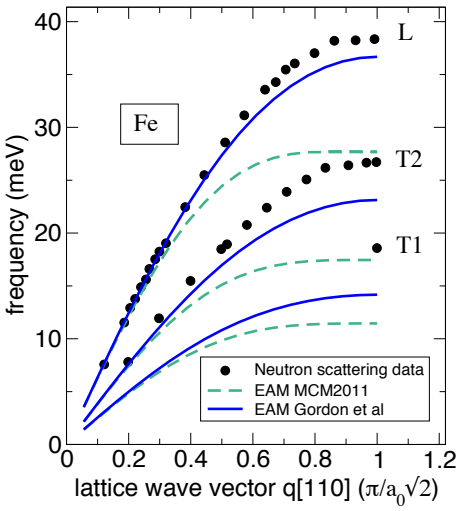

FIG. 3. Phonon band along the [110] direction with different EAM models (see legend) and neutron scattering data (symbols) from Ref. [10] in Supplementary bibliography.

predictions for the Peierls stress, about 0.2 GPa, remains smaller than the quantum effect evidenced in the present study, since the latter yields a quantum Peierls stress more than 0.4 GPa below the classical Peierls stress.

In order to rationalize the discrepancy of 0.2 GPa between the two EAM potentials, one should first note that the classical Peierls stress is 0.9 GPa with Gordon potential, which is 0.15 GPa smaller than with MCM2011. While such a difference is related to the difference in Peierls potentials predicted by both potentials (see Fig. 1), the rest of the difference can be ascribed to the vibrational modes, which also differs in the two models. We have reported in Supplementary Fig. 3 the phonon frequency spectrum along the [110] direction in a perfect iron crystal, computed with both iron models, along with experimental data. The difference between the two models appears clearly at the edge of the phonon bands for longitudinal (L) and transversal (T) modes. Gordon potential follows more closely neutron scattering experimental data (Ref. [10] in Supplementary bibliography). This actually orientated our choice about which Fe model to employ to capture accurately the crystal vibrational modes.

In conclusion, both EAM iron models present qualities and drawbacks on various respects. MCM2011 is accurate for the screw dislocation Peierls potential but does not reproduce correctly the phonon frequency spectrum at high frequencies. On the opposite, Gordon potential is more accurate for the phonon spectrum but reproduces less correctly the Peierls potential profile. At the stage of the present work, it has not been possible to adjust an EAM potential in order to obtain satisfactory accuracy on both aspects, but the fact that in both cases, the quantum Peierls stress is strongly reduced with respect to the classical Peierls stress, confirms the robustness of the result presented in the main article.

Supplementary bibliography

[1] V. Benderskii, D. Makarov, and C. Wight, *Chemical Dynamics at Low Temperature* (Wiley-Interscience, New York, 1994)

[2] W. Miller, *Semiclassical limit of quantum mechanical transition state theory for nonseparable systems,* J. Chem. Phys. **62**, 1899-1906 (1975)

[3] L. Landau and E. Lifshitz, *Quantum mechanics Non-Relativistic theory* (Elsevier Science Ltd., Oxford, 1977)

[4] M. Gillan, *Quantum-classical crossover of the transition rate in the damped double well,* J. Phys. C **20**, 3621 (1987)

[5] N. Ashcroft and N. Mermin, *Solid State Physics* (Saunders College Publishing, 1976)

[6] M. Daw, S. Foiles, and M. Baskes, *The embedded-atom method: a review of theory and applications,* Mat. Sci. Rep. **9**, 251-310 (1993)

[7] M. Mendelev, S. Han, D. Srolovitz, G. Ackland, D. Sun, and M. Asta, *Development of new interatomic potentials appropriate for crystalline and liquid iron,* Philos. Mag. **83**, 3977-3994 (2003)

[8] P.A. Gordon, T. Neeraj, M.I. Mendelev *Screw dislocation mobility in BCC Metals: a refined potential description for α-Fe,* Philos. Mag. Lett. **91**, 3931-3945 (2011)

[9] L. Ventelon and F. Willaime, *Core structure and Peierls potential of screw dislocations in α-Fe from first principles: cluster versus dipole approaches,* J. Comput.-aided Mat. Design **14**, 85 (2007)
[10] V. J. Minkiewicz, G. Shirane, and R. Nathans, *Phonon dispersion relation for iron,* Phys. Rev. **162**, 528-531 (1967)